nature communications

Article

https://doi.org/10.1038/s41467-025-64555-z

Charge transfer governed interlayer magnetic coupling and symmetry breaking in a van der Waals magnet

Received: 14 May 2025

Accepted: 19 September 2025

Canyu Hong[1,8], Zeyuan Sun[1,2,3,8] ✉, Zhiyuan Sheng[1], Shuang Wu[1], Yi Chen[4], Ming Tian[5], Neng Wan[1,5], Qixi Mi[4], Zhongkai Liu[4], Weibin Chu[6] & Shiwei Wu[1,2,3,7] ✉

Van der Waals (vdW) magnets provide a rich landscape for innovative spintronic applications at atomic thickness. Among them, chromium sulfide bromide (CrSBr) stands out as a semiconducting antiferromagnet with the potential for magnetoelectric manipulation. However, the detection and electrical control of 2D magnetism in CrSBr are constrained by its centrosymmetric structure and in-plane antiferromagnetism. To address this challenge, we construct heterostructure devices composed of trilayer CrSBr and monolayer graphene, where interfacial charge transfer breaks the inversion symmetry of both magnetic order and crystallographic structure. The inversion symmetry breaking by charge transfer thus allows a full discrimination of the otherwise degenerate magnetic states using optical second harmonic generation, including the charge transfer induced intermediate magnetic states that consist of antiferromagnetic and ferromagnetic vdW interfaces. Furthermore, gate voltage enables the tuning of charge transfer, effectively modulating the interlayer magnetic coupling and magnetic transitions. Our findings deepen the understanding of optospintronic interaction and magnetoelectric manipulation in vdW magnets, paving the way for electrically tunable 2D spintronic devices.

Two-dimensional (2D) semiconducting magnets, in conjunction with the possibility to engineer homo- or hetero-structures, provide a promising platform for realizing magnetoelectric coupling and spin-based functionalities[1–8]. A notable example of such 2D semiconducting magnets is chromium sulfide bromide (CrSBr)[9–11]. Its strong coupling between magnetism and semiconducting band structure gives rise to emergent phenomena such as exciton-magnon coupling[12–14] and exciton polaritons[15,16], and allows the construction of heterostructures for transport studies[17,18]. Despite the great potential of CrSBr, its centrosymmetric lattice structure and in-plane layered antiferromagnetism severely limit the effective characterization and control of the magnetic states[9,10,19]. Although nonlinear optical techniques can probe magnetic states in even-layer CrSBr with noncentrosymmetric magnetic order[20], odd-layer CrSBr remains experimentally inaccessible because of the centrosymmetric antiferromagnetic (AFM) and ferromagnetic (FM) spin configurations. Overcoming this limitation

---

[1]State Key Laboratory of Surface Physics and Department of Physics, Fudan University, Shanghai, China. [2]Institute for Nanoelectronic Devices and Quantum Computing, Fudan University, Shanghai, China. [3]Key Laboratory of Micro and Nano Photonic Structures (MOE), Fudan University, Shanghai, China. [4]School of Physical Science and Technology, ShanghaiTech Laboratory for Topological Physics, ShanghaiTech University, Shanghai, China. [5]Key Laboratory of MEMS of the Ministry of Education, School of Integrated Circuit, Southeast University, Nanjing, China. [6]Key Laboratory of Computational Physical Sciences (MOE), and Institute of Computational Physical Sciences, Fudan University, Shanghai, China. [7]Shanghai Research Center for Quantum Sciences, Shanghai, China. [8]These authors contributed equally: Canyu Hong, Zeyuan Sun. ✉e-mail: zysun@fudan.edu.cn; swwu@fudan.edu.cn

requires an external symmetry-breaking mechanism to probe and control the intricate magnetic evolutions.

In this work, we study the magnetic transition behavior in gated trilayer (3L) CrSBr devices using magneto-photoluminescence (PL) and magnetic second harmonic generation (SHG). The devices are constructed as heterostructures comprising 3L CrSBr and monolayer graphene in a back-gate geometry. Between 140 K and 40 K, we observe conventional magnetic transitions between AFM and FM states under an external magnetic field along the easy axis. Remarkably, below 40 K, a new type of intermediate magnetic states emerges, which is attributed to the charge transfer induced modulation of interlayer AFM coupling. Furthermore, while the crystallographic and magnetic structures of bare 3L CrSBr are centrosymmetric, the graphene-covered heterostructure and ensuing charge transfer break the inversion symmetry of both lattice structure and magnetic order, which enables the electric-dipole (ED) allowed time invariant (i-type) and noninvariant (c-type) contributions to SHG. The symmetry-sensitive SHG not only reveals the coexistence of FM and AFM vdW interfaces within the new intermediate states, which are called “Mixed states”, but also allows the differentiation of the otherwise degenerate AFM and FM states. By further modulating the back-gate voltage, we achieve the control of interlayer exchange interactions, thus tailoring the evolution of magnetic transitions. Our study offers new insights and methodologies for the exploration of 2D magnets and their prospective applications in functional spintronic devices.

Results

Magnetic hysteresis switching in trilayer CrSBr devices

Figure 1a shows the structure of a 3L CrSBr back-gate device. The 3L CrSBr is covered by a monolayer graphene, which also contacts the two gold (Au) electrodes positioned on either side of the CrSBr. These electrodes allow to monitor the charge neutral point in graphene. A thin flake of hexagonal boron nitride (hBN) is encapsulated on top of the graphene/CrSBr heterostructure as a protective capping layer. Since the exchange interaction in CrSBr is highly sensitive to strain[21], the 3L CrSBr is exfoliated directly onto the substrate without any pickup process during dry transfer. This approach minimizes strain-induced inhomogeneity in the CrSBr. The entire exfoliation and encapsulation are performed in a glove box under a nitrogen atmosphere to prevent potential contamination of the sample.

The coupling of magnetic structures and exciton emission in CrSBr allows for the investigation of magnetic transitions via PL characterization[10,18,22]. We first employ magneto-PL measurements at various temperatures. Figure 1b, c present the PL intensity loops as the magnetic field sweeps from −0.4 T to 0.4 T (forward) and vice versa (backward) along the easy axis (***b***-axis), across a temperature range from 200 K to 7 K. The PL intensity is integrated from the exciton emission within the energy range from 1.24 eV to 1.38 eV. To highlight the intensity switching, the temperature-dependent PL loops are normalized by using the intensity difference between 0 T and 0.4 T at 7 K (see Supplementary Fig. 1 and Supplementary Note 1). Above the Néel temperature (T_N) at ~135 K[9,10,19,23,24], the 3L CrSBr exhibits a paramagnetic state, with no PL intensity switching observed during magnetic field sweeps. Between 135 K and 40 K, the PL loops reveal two distinct intensity levels, as demonstrated by a representative loop at 75 K in Fig. 1d. These levels correspond to different magnetic states, with layered AFM states appearing at low magnetic fields and FM states emerging at high fields[10,20].

Notably, a new lower-intensity level emerges below 40 K, as illustrated by the loop at 7 K (Fig. 1e). To further differentiate the three PL intensity levels in 3L CrSBr device, we obtain the excitonic PL spectra. As depicted in Fig. 2a, the spectra at ±0.4 T exhibit a single excitonic peak at 1.328 eV. At 0 T, the PL spectra display two separate excitonic peaks at 1.338 eV and 1.363 eV. These observations are consistent with previous studies[10,22], where the spectra at ±0.4 T correspond to FM states and those at 0 T correspond to AFM states. By contrast, the spectra at ±0.2 T both show a single peak at 1.338 eV, which differ from those of the FM and AFM states. The corresponding PL images confirm the uniformity and high quality of our samples (Fig. 2a, insets). These observations suggest that the new PL level corresponds to an unidentified type of magnetic states. The PL results are reproduced in an additional 3L CrSBr device S2, as shown in Supplementary Fig. 2.

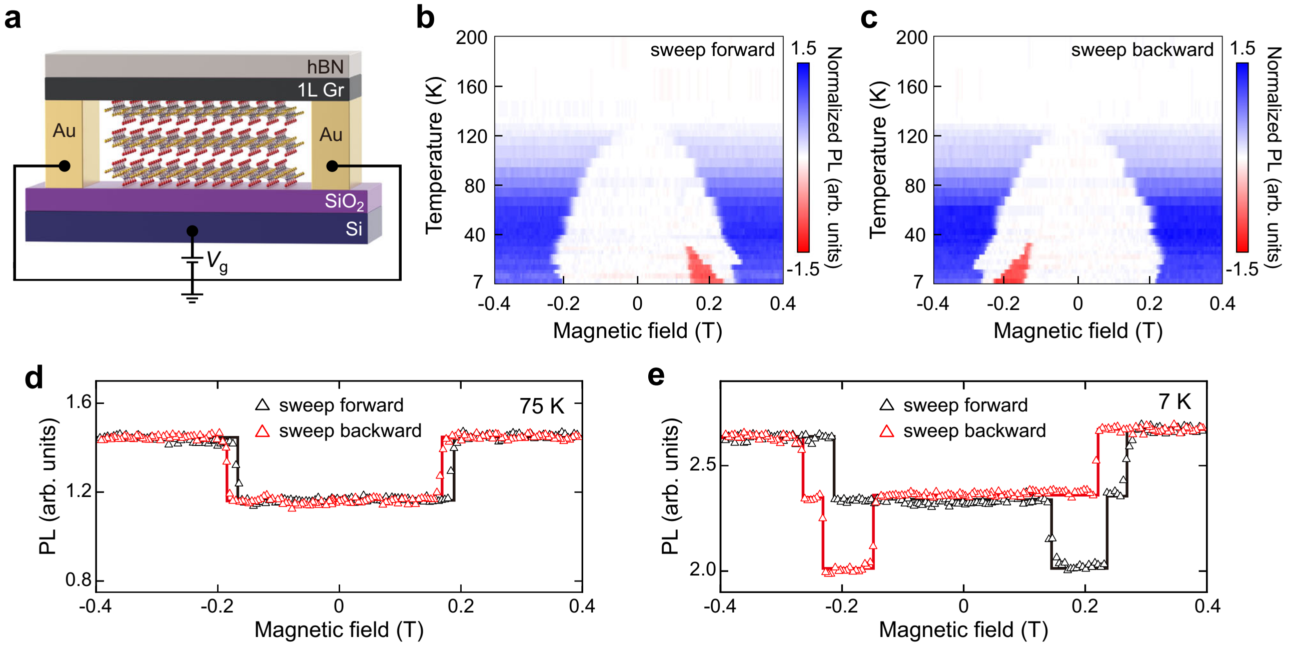

Fig. 1 | Magneto-PL measurements of 3L CrSBr device. a Schematic of 3L CrSBr device. The monolayer graphene (1L Gr) is contacted with two Au electrodes for monitoring its charge neutral point. The back gate voltage (V_g) is applied to the silicon substrate. Temperature dependent PL intensity loops from 200 K to 7 K, with the magnetic field sweeping forward (**b**) and backward (**c**) along the easy axis. The PL intensity is normalized as detailed in Supplementary Note 1. PL hysteresis loops at 75 K (**d**) and 7 K (**e**).

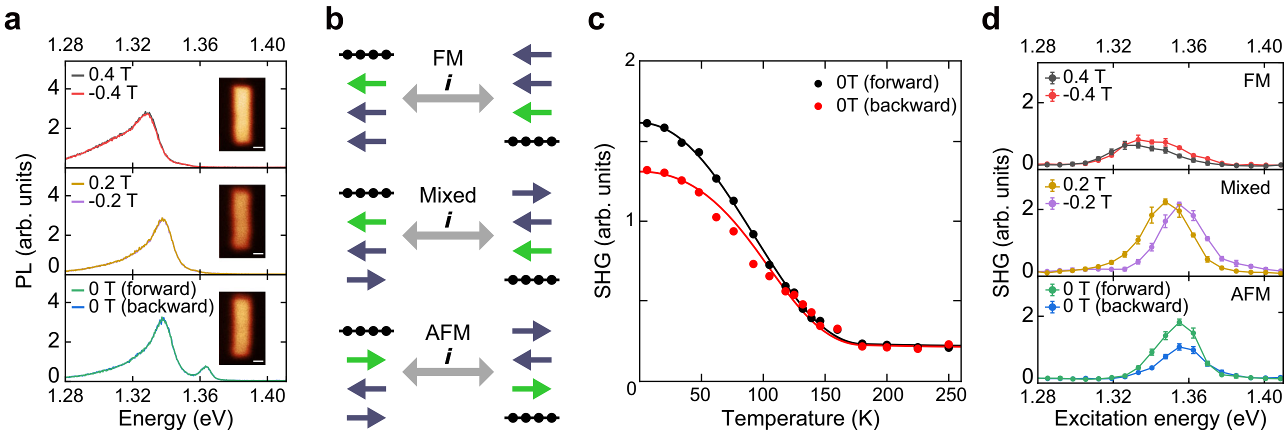

Fig. 2 | Magnetic SHG of the 3L CrSBr device. a PL spectra at ±0.4 T (top), ±0.2 T (middle) and ±0 T (bottom), respectively. The insets are the corresponding PL microscopic images. Scale bar, 2 μm. **b** Symmetry analysis of the lattice structure and the FM (top), Mixed (middle), and AFM (bottom) structures of 3L CrSBr. The spatial-inversion operation is denoted by the symbol ***i***. The CrSBr layer with charge transfer from the contacted graphene is marked by the green arrows. The charge transfer breaks the inversion symmetry of the lattice and FM, Mixed, and AFM states under the spatial-inversion operation ***i***. **c** Temperature dependence of SHG intensity for the two AFM states. The red and black solid curves are shown as a guide for the eye. **d** SHG excitation spectra at ±0.4 T (top), ±0.2 T (middle), and ±0 T (bottom), respectively.

To better understand the emergent states, we categorize all possible magnetic structures, as summarized in Supplementary Table 1. The magnetic states can be classified into three types based on interfacial magnetization: FM states (**M** = ±3) with two FM vdW interfaces, AFM states (**M** = ±1) with two AFM interfaces, and Mixed states (**M** = ±1) with one FM and one AFM interfaces. Here, **M** denotes the total magnetization of the three CrSBr layers, where the magnetization in each monolayer is represented by left and right arrows, corresponding to **M** = −1 and 1, respectively. Within each category, the magnetic configurations share equivalent interlayer magnetic arrangements, resulting in identical excitonic PL emission. Thus, the three types of PL spectra can be attributed to the FM, Mixed and AFM states, with the states at ±0.2 T reasonably assigned to the Mixed states.

Note that the Mixed state is absent in a bare 3L CrSBr, where only two PL levels corresponding to the AFM and FM states are observed (Supplementary Fig. 3). In contrast, the Mixed state emerges when 3L CrSBr is covered with graphene, highlighting the crucial role of the heterostructure interface. Theoretical calculation indicates significant charge transfer occurring between graphene and CrSBr[25], which weakens the interlayer AFM coupling of the top two CrSBr layers, thereby facilitating the formation of the Mixed state.

Symmetry breaking of magnetic states in trilayer CrSBr devices

Charge transfer not only leads to the emergence of the Mixed state, but also breaks the inversion symmetry of the electronic structures associated with the lattice and magnetic orders in the heterostructure. In bare 3L CrSBr, both the crystallographic structure and the AFM/FM magnetic configurations are centrosymmetric, while inversion symmetry is broken only in the Mixed state. In contrast, in the graphene/CrSBr heterostructure (Fig. 2b), charge transfer from the contacted graphene induces doping of the top CrSBr layer (as indicated by the green arrows), which breaks the inversion symmetry of both crystallographic structure and all three types of magnetic structures. This symmetry breaking enables the electric-dipole allowed second harmonic generation (ED-SHG), which is a powerful nonlinear optical technique for characterizing both crystallographic structures and magnetic orders[19,20,26–28]. Thus, the graphene/CrSBr heterostructure provides an ideal platform to explore charge-doping-induced ED-SHG arising from both the lattice and magnetism.

Specifically, the SHG from the crystallographic and magnetic structures is described by the time-invariant tensor χ_i and the time-noninvariant tensor χ_c, respectively[26]. Under time-reversal operation, χ_i remains unchanged while χ_c changes sign. The existence of χ_i and χ_c is experimentally evidenced by the temperature-dependent SHG measurements, as shown in Fig. 2c. At low temperature, the SHG intensity measured at two AFM states shows clear differences, which arise from the coherent superposition of the lattice (χ_i) and magnetic (χ_c) contributions. This distinction is a direct consequence of the fact that χ_c changes sign between two time-reversal AFM states, while χ_i remains unchanged. As the temperature increases, both SHG intensities at two AFM states gradually decrease but remain non-zero at the paramagnetic state above T_N, indicating the χ_i contribution from the inversion-symmetry breaking of the crystallographic structure.

To further demonstrate the interference between lattice and magnetism, the polarization-resolved SHG patterns of the AFM and Mixed states are acquired (see Supplementary Fig. 4). The patterns are well fitted by the interference of SHG contribution from χ_i and χ_c, which are based on crystallographic point group 2 and magnetic point group $\underline{m}m\underline{m}$, respectively (see Supplementary Note 2 for detailed analysis). This interference is also reflected in the SHG spectra, as shown in Fig. 2d. At two FM states (±0.4 T), the SHG spectra exhibit broad resonance peaks around 1.340 eV with distinct intensity. For the two AFM states, the resonance peaks shift and become more prominent at 1.355 eV, again with different intensity. These results are consistent with the interference between SHG contributions from χ_i and χ_c. As the magnetic structures transition to the Mixed states at ±0.2 T, the resonance peaks remarkably split into two energies of nearly equal intensity. This energy splitting originates from the breaking of PT symmetry by the magnetic structure of Mixed states, which lifts the Kramers-like degeneracy and leads to distinct resonance energies[29]. Since the AFM and FM states in bare CrSBr are intrinsically PT symmetric, the inversion symmetry breaking induced by charge doping is not so obvious. In contrast, the Mixed states intrinsically lack PT symmetry, giving rise to a more pronounced energy splitting in the SHG spectra.

Building on this understanding, the charge-transfer-induced lifting of degeneracy in the SHG excitation spectra provides an effective approach for differentiating all six magnetic states at a specific photon energy. Figure 3a shows the SHG hysteresis loop measured at an excitation photon energy of 1.355 eV. Five distinct plateaus are observed in the SHG loop during a unidirectional magnetic field sweep. Unlike the PL loop, the two AFM states at zero magnetic field can be distinguished by their SHG intensity. The Mixed states at ±0.2 T also

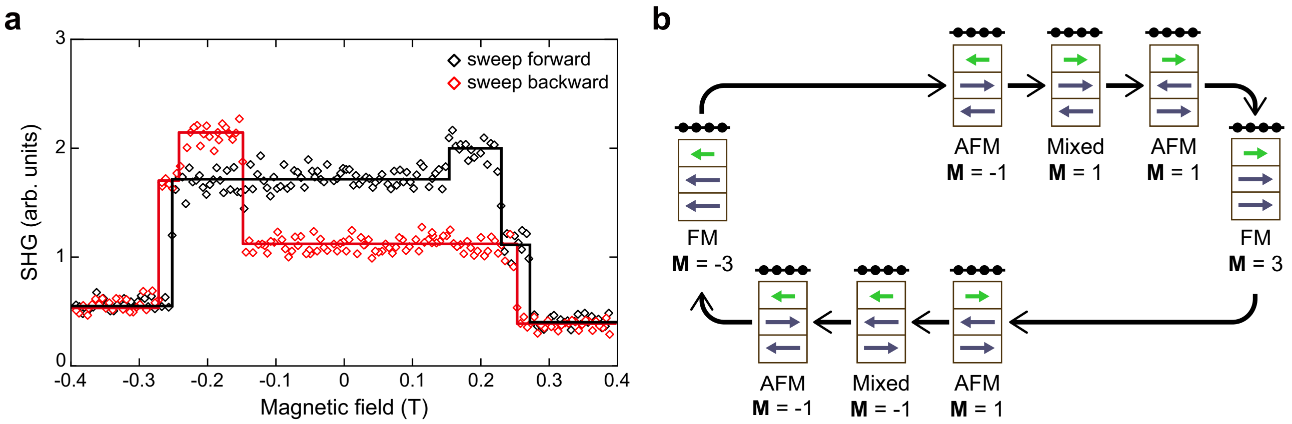

Fig. 3 | SHG hysteresis loop and the magnetic evolution. **a** SHG hysteresis loop measured using the excitation photon energy of 1.355 eV. **b** Magnetic evolution for the 3L CrSBr device. The electron doping from graphene (black dots and lines) modulates the contacted CrSBr layer, as indicated by green arrows.

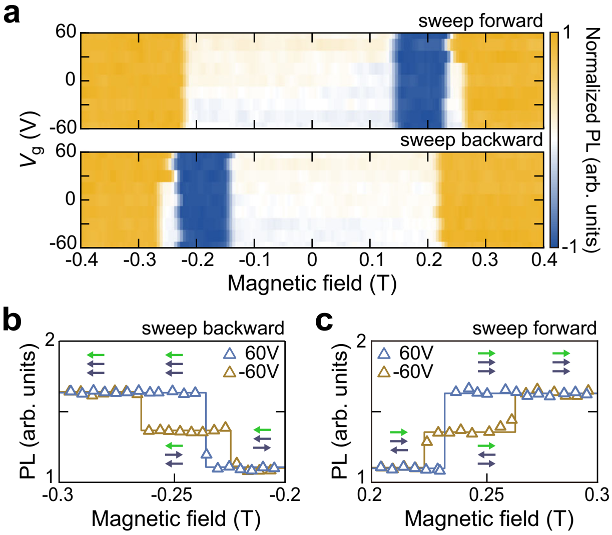

Fig. 4 | Gate-tunable magnetic transitions for the 3L CrSBr device. **a** Magneto-PL loops under different gate voltages. Zoomed-in PL intensity from the Mixed states to FM states during the backward (**b**) and forward (**c**) sweeps at $V_g = \pm 60$ V. The insets show the magnetic structures corresponding to the PL intensity plateaus. Compared to $V_g = -60$ V, the middle plateau corresponding to the AFM states disappears at $V_g = 60$ V.

show SHG intensity differences, which become more pronounced at various excitation energies (Supplementary Fig. 5). Significantly, the SHG intensity differs between the two states that switch before and after the Mixed states, confirming that they correspond to two time-reversal AFM states. The FM states at ±0.4 T also exhibit intensity differences in their SHG responses.

Consequently, we outline the magnetic evolution of 3L CrSBr, as illustrated in Fig. 3b. In the forward sweep, the magnetic structure begins in the FM state ($\mathbf{M} = -3$) under magnetic field of −0.4 T. As field sweeps to 0 T, a spin-flip transition occurs in the middle layer, driven by the interlayer AFM coupling from the two vdW interfaces, leading to the AFM state ($\mathbf{M} = -1$). With further increases in magnetic field, the 3L CrSBr transitions to the Mixed state ($\mathbf{M} = 1$). Notably, the charge transfer from graphene to 3L CrSBr leads to the reduction of the interlayer AFM coupling between the upper two CrSBr layers[25], thereby promoting the formation of the Mixed state, in which the upper two layers become ferromagnetically coupled. In contrast, the spatial-inversion or time-reversal counterparts of this Mixed state, which require either flipping the bottom layer or simultaneously flipping the bottom two layers of the AFM state ($\mathbf{M} = -1$) (Supplementary Table 1), remains energetically unfavorable under the sample geometry.

Subsequently, the trilayer CrSBr switches to the AFM state with $\mathbf{M} = 1$ within a small field range near 0.25 T. This state is the time-reversal counterpart of the AFM state at 0 T (forward), which is intensity degenerate in PL measurements. The wavelength-dependent SHG measurements further distinguish these two states (Supplementary Fig. 5). Opposite transition behaviors are observed during the backward sweep from 0.4 T to −0.4 T, which exhibit a time-reversal evolution of the magnetic structures compared to the forward sweep. For comparison, an SHG loop of a bare 3L CrSBr is shown in Supplementary Fig. 6, which exhibits vanished SHG intensity due to the centrosymmetric magnetic structure of intrinsic AFM and FM states.

Gate-tunable magnetic transitions

The well-defined magnetic structures in the 3L CrSBr device allow us to study the magnetic transition behavior under variable gate voltages.

Figure 4a displays the PL intensity loops across various gate voltages between ±60 V, with the magnetic field sweeps shown for both forward (upper panel) and backward (lower panel) directions. Interestingly, the transitions from the Mixed states to the FM states is significantly influenced by the gate voltages. Figure 4b, c present the zoomed-in magneto-PL data, focusing on the magnetic field range where the Mixed states switch to the FM states. Under positive gate voltages, the Mixed states transition directly to the FM states. By contrast, under negative gate voltages, the Mixed states undergo two-step transitions: first to the AFM states and then to the FM states. It is worth noting that the Fermi level of the graphene/3L CrSBr heterostructure is characterized to be nearly aligned with the Dirac point of the graphene (Supplementary Fig. 7). Accordingly, the CrSBr layer in contact with graphene is under the electron doping density of ~2.0×10^{13} cm^{-2}[25,30], which arises from the Dirac point of graphene being ~0.5 eV higher than the conduction band minimum of CrSBr. In contrast, the maximum charge density induced by a 60 V back-gate voltage is only ~4.7×10^{12} cm^{-2}, so that the CrSBr is always under the electron-doped regime throughout this study.

To analyze the gate-controlled magnetic transitions, a simplified linear chain model is used to simulate the delicate energy balance within the magnetic evolution. In brief, the gate-controlled charge transfer effectively modulates the relative strength of interlayer exchange interactions, thereby tuning the spin-flipping sequence and determining the observed magnetic transition behavior (see details in Supplementary Note 3). For clarity, the three layers from the bottom to the top are labeled as layer 1, layer 2, and layer 3, respectively. The electrostatic doping in layer 3, which is induced by the gate voltage, modulates the interlayer exchange interaction J_{23} between the top two CrSBr layers. Specifically, J_{23} decreases under positive gate voltages and increases under negative voltages. At positive gate voltages, the reduction in J_{23} allows the magnetic anisotropy energy K of layer 2 to play a dominant role in stabilizing its spin orientation. As a result, the 3L CrSBr device undergoes a direct transition from the Mixed state to the FM state, with only layer 1 flipping. By contrast, at negative gate voltages, the increased interlayer AFM coupling between layers 2 and 3 favors the simultaneous flipping of layers 1 and 2 before reaching the FM state. Consequently, an intermediate AFM state between the Mixed state and the FM state appears during the magnetic evolution.

Discussion

Our results demonstrate that the charge transfer serves as an effective mechanism for modulating the interlayer exchange interaction in 3L CrSBr. The influence of charge transfer occurs exclusively at temperatures below 40 K, which is associated with the emergence of the Mixed states. This phenomenon can be interpreted as increased localization of intralayer electronic states below 40 K, leading to the suppression of interlayer carrier hopping. Consequently, the confinement of doped carriers within the top CrSBr layer enhances the doping effect and thus weakens the AFM coupling between the top two CrSBr layers. The observed transition temperature of 40 K is consistent with previous reports from magnetic susceptibility, electrical, optical, and thermal transport studies on bulk and few-layer CrSBr[22–24,31,32], where these phenomena have been attributed to magnetic defects[22,24,31] and spin freezing[23,32].

In summary, we observe a new intermediate magnetic state in 3L CrSBr devices below 40 K, which is conclusively demonstrated by the coexistence of AFM and FM vdW interfaces, as characterized by PL measurements. The emergence of this state is attributed to charge transfer from the covered monolayer graphene to 3L CrSBr, which modulates the interlayer AFM coupling between the upper two CrSBr layers. The charge transfer also breaks the inversion symmetry of both crystallographic and magnetic structures of 3L CrSBr, leading to the interference between the two SHG contributions, which lifts the degeneracy of time-reversal magnetic counterparts. Furthermore, the magnetic transitions can be controlled by gate voltage via tuning the doping density. These findings highlight that interfacial charge transfer in 2D heterostructures provides a versatile means of controlling magnetism, symmetry, and optical responses. Given that charge transfer commonly occurs and can be readily induced in a broad range of vdW assemblies, this mechanism offers a general strategy for tuning the functionalities of various 2D materials.

Methods

Device fabrication

CrSBr crystals were grown in a quartz tube charged with Cr powder and S_2Br_2 and characterized by single-crystal X-ray diffraction[20]. The hBN crystals used in this study were grown by Southeast University using the atmospheric-pressure high-temperature method[33]. CrSBr trilayers were mechanically exfoliated onto 285 nm SiO_2/Si substrate using Nitto tape. The thickness of the CrSBr flakes was determined by the optical contrast method in combination with atomic force microscopy. A conventional dry transfer process was employed to assemble hBN/graphene/CrSBr heterostructure. To minimize strain on the CrSBr, the CrSBr was avoided from being picked up during the dry transfer process. All fabrication procedures were performed in a nitrogen atmosphere, except for the dissolution of residual polycarbonate in tetrachloromethane solution for a few seconds. The devices were then transferred to the magneto-optical cryostat under nitrogen protection. These approaches minimize the strain-induced spatial inhomogeneity and contamination.

Optical measurements

All measurements were conducted using our home-built cryogen-free variable temperature magneto-optical microscope down to ~7 K. This system is equipped with a room-temperature-bore 3-axis superconducting magnet, and the crystal axes of 3L CrSBr were visually aligned to the vector magnet axis. Additionally, the system features a reflective confocal microscope with an objective of numerical aperture of 0.55. The confocal microscope is equipped with piezo-actuated positioning and scanning stages for locating the sample position and acquiring signal mapping. The gate voltage was applied to the SiO_2/Si substrate with a Source/Meter Unit (Keithley) while acquiring the optical signal.

PL was excited at 632.8 nm and ~12 μW with a He-Ne laser (Thorlabs). The spot size was 1 μm. The excitation polarization was tuned along the ***b***-axis of the CrSBr crystal, and the signal collection polarization was aligned accordingly. The magneto-PL intensity was collected with an avalanche photodiode (Perkin Elmer) via a low-hydroxyl infrared optical fiber, utilizing an optical filter to select the energy range (from 1.24 eV to 1.38 eV). PL spectra were resolved by an HRS-500MS spectrometer with a 150 g/mm grating and a PYL-100BRX CCD from Princeton Instruments.

For SHG measurements, a femtosecond OPO laser (Spectra Physics) was used to provide the excitation pulse laser with a duration of ~120 fs. The signal detection was performed using a photon-counting photomultiplier tube (Hamamatsu). The SHG excitation power was maintained at ~200 μW for all wavelengths. To obtain the polarization-resolved SHG patterns, the polarization of the incident beam was rotated using a half-wave plate, and the SHG signal was detected after passing through the same half-wave plate and a linear polarizer oriented perpendicular to the incident polarization. These polarization-dependent data were acquired by recording a series of polarization-resolved SHG images at different azimuthal angles. For all other SHG measurements, the excitation polarization was aligned along the ***b***-axis, while the signal polarization was set perpendicular to it.

Data availability

The data supporting the findings of this study are available within the paper. Source data are provided with this paper.

References

1. Song, T. et al. Giant tunneling magnetoresistance in spin-filter van der Waals heterostructures. *Science* **360**, 1214–1218 (2018).
2. Klein, D. R. et al. Probing magnetism in 2D van der Waals crystalline insulators via electron tunneling. *Science* **360**, 1218–1222 (2018).
3. Wang, Z. et al. Very large tunneling magnetoresistance in layered magnetic semiconductor CrI_3. *Nat. Commun.* **9**, 2516 (2018).
4. Huang, B. et al. Electrical control of 2D magnetism in bilayer CrI_3. *Nat. Nanotechnol.* **13**, 544–548 (2018).
5. Jiang, S., Li, L., Wang, Z., Mak, K. F. & Shan, J. Controlling magnetism in 2D CrI_3 by electrostatic doping. *Nat. Nanotechnol.* **13**, 549–553 (2018).
6. Jiang, S., Li, L., Wang, Z., Shan, J. & Mak, K. F. Spin tunnel field-effect transistors based on two-dimensional van der Waals heterostructures. *Nat. Electron.* **2**, 159–163 (2019).
7. Wang, Q. et al. The magnetic genome of two-dimensional van der Waals materials. *ACS Nano* **16**, 6960–7079 (2022).
8. Chen, Y. et al. Twist-assisted all-antiferromagnetic tunnel junction in the atomic limit. *Nature* **632**, 1045–1051 (2024).
9. Telford, E. J. et al. Layered antiferromagnetism induces large negative magnetoresistance in the van der Waals semiconductor CrSBr. *Adv. Mater.* **32**, 2003240 (2020).
10. Wilson, N. P. et al. Interlayer electronic coupling on demand in a 2D magnetic semiconductor. *Nat. Mater.* **20**, 1657–1662 (2021).
11. Ziebel, M. E. et al. CrSBr: An air-stable, two-dimensional magnetic semiconductor. *Nano Lett.* **24**, 4319–4329 (2024).
12. Bae, Y. J. et al. Exciton-coupled coherent magnons in a 2D semiconductor. *Nature* **609**, 282–286 (2022).
13. Diederich, G. M. et al. Tunable interaction between excitons and hybridized magnons in a layered semiconductor. *Nat. Nanotechnol.* **18**, 23–28 (2023).
14. Sun, Y. et al. Dipolar spin wave packet transport in a van der Waals antiferromagnet. *Nat. Phys.* **20**, 794–800 (2024).
15. Dirnberger, F. et al. Magneto-optics in a van der Waals magnet tuned by self-hybridized polaritons. *Nature* **620**, 533–537 (2023).
16. Ruta, F. L. et al. Hyperbolic exciton polaritons in a van der Waals magnet. *Nat. Commun.* **14**, 8261 (2023).
17. Ghiasi, T. S. et al. Electrical and thermal generation of spin currents by magnetic bilayer graphene. *Nat. Nanotechnol.* **16**, 788–794 (2021).
18. Tabataba-Vakili, F. et al. Doping-control of excitons and magnetism in few-layer CrSBr. *Nat. Commun.* **15**, 4735 (2024).
19. Lee, K. et al. Magnetic order and symmetry in the 2D semiconductor CrSBr. *Nano Lett.* **21**, 3511–3517 (2021).
20. Sun, Z. et al. Resolving and routing magnetic polymorphs in a 2D layered antiferromagnet. *Nat. Mater.* **24**, 226–233 (2025).
21. Cenker, J. et al. Reversible strain-induced magnetic phase transition in a van der Waals magnet. *Nat. Nanotechnol.* **17**, 256–261 (2022).
22. Marques-Moros, F., Boix-Constant, C., Mañas-Valero, S., Canet-Ferrer, J. & Coronado, E. Interplay between optical emission and magnetism in the van der Waals magnetic semiconductor CrSBr in the two-dimensional limit. *ACS Nano* **17**, 13224–13231 (2023).
23. López-Paz, S. A. et al. Dynamic magnetic crossover at the origin of the hidden-order in van der Waals antiferromagnet CrSBr. *Nat. Commun.* **13**, 4745 (2022).
24. Telford, E. J. et al. Coupling between magnetic order and charge transport in a two-dimensional magnetic semiconductor. *Nat. Mater.* **21**, 754–760 (2022).
25. Xie, K., Zhang, X.-W., Xiao, D. & Cao, T. Engineering magnetic phases of layered antiferromagnets by interfacial charge transfer. *ACS Nano* **17**, 22684–22690 (2023).
26. Fiebig, M., Fröhlich, D., Krichevtsov, B. B. & Pisarev, R. V. Second harmonic generation and magnetic-dipole-electric-dipole interference in antiferromagnetic Cr_2O_3. *Phys. Rev. Lett.* **73**, 2127–2130 (1994).
27. Sun, Z. et al. Giant nonreciprocal second-harmonic generation from antiferromagnetic bilayer CrI_3. *Nature* **572**, 497–501 (2019).
28. Shen, Y. R. *Second Harmonic and Sum-frequency Spectroscopy: Basics and Applications* (World Scientific, 2023).
29. Chen, H. et al. Basic formulation and first-principles implementation of nonlinear magneto-optical effects. *Phys. Rev. B* **105**, 075123 (2022).
30. Rizzo, D. J. et al. Engineering anisotropic electrodynamics at the graphene/CrSBr interface. *Nat. Commun.* **16**, 1853 (2025).
31. Klein, J. et al. Sensing the local magnetic environment through optically active defects in a layered magnetic semiconductor. *ACS Nano* **17**, 288–299 (2023).
32. Canetta, A. et al. Impact of spin-entropy on the thermoelectric properties of a 2D magnet. *Nano Lett.* **24**, 6513–6520 (2024).
33. Sheng, Z. et al. Dielectric breakdown of atmospheric-pressure grown hexagonal boron nitride single crystals. *Appl. Phys. Lett.* **126**, 233102 (2025).

Acknowledgements

The work at Fudan University was supported by National Natural Science Foundation of China (Grant Nos. 12034003, 12427807), National Key Research and Development Program of China (Grant Nos. 2022YFA1403302, 2024YFA1409800), Science and Technology Commission of Shanghai Municipality (Grant Nos. 23JC1400400, 2019SHZDZX01), Shanghai Municipal Education Commission (Grant No. 2021KJKC-03-61). Z.L. acknowledges the support from the National Natural Science Foundation of China (Grant Nos. 92365204, 12274298) and the National Key Research and Development program of China (Grant No. 2022YFA1604403).

Author contributions

S.W.W. conceived and supervised the project. C.H. and Z.Y. Sun performed the experiments with assistance from Z.Y. Sheng and S.W. Y.C., Q.M., and Z.L. provided the CrSBr single crystals. M.T. and N.W. provided the hBN single crystals. W.B.C. helped analyze the excitonic states. Z.Y. Sun carried out a numerical simulation of the linear chain model. C.H., Z.Y. Sun and S.W.W. analyzed the data and wrote the paper with inputs from all the authors.

Competing interests

The authors declare no competing interests.

Additional information

Supplementary information The online version contains supplementary material available at https://doi.org/10.1038/s41467-025-64555-z.

Correspondence and requests for materials should be addressed to Zeyuan Sun or Shiwei Wu.

Peer review information *Nature Communications* thanks the anonymous reviewers for their contribution to the peer review of this work. A peer review file is available.